Photoexcitation electron paramagnetic resonance studies on nickel-related defects in diamond

2003 J. Phys.: Condens. Matter 15 2493

(http://iopscience.iop.org/0953-8984/15/17/305)

INSTITUTE OF PHYSICS PUBLISHING JOURNAL OF PHYSICS: CONDENSED MATTER

J. Phys.: Condens. Matter **15** (2003) 2493–2505 PII: S0953-8984(03)57431-8

Photoexcitation electron paramagnetic resonance studies on nickel-related defects in diamond

R N Pereira[1,2,3], **W Gehlhoff**[2], **A J Neves**[1] **and N A Sobolev**[1]

[1] Departamento de Física, Universidade de Aveiro, 3810-193 Aveiro, Portugal
[2] Institut für Festkörperphysik, Technische Universität Berlin, 10623 Berlin, Germany

E-mail: pereira@phys.au.dk

Received 13 December 2002
Published 22 April 2003
Online at stacks.iop.org/JPhysCM/15/2493

Abstract

Measurements of the electron paramagnetic resonance (EPR) upon photoexcitation are reported on Ni defects in diamonds grown with Ni-containing solvent/catalysts. The temperature dependence of the W8 EPR spectrum photoquenching shows that the relaxation of substitutional Ni_s^- upon electron ionization is very small, corroborating the interpretation that the previously reported photoinduced effects with thresholds at 2.5 and 3.0 eV correspond to two complementary photoionization transitions involving Ni_s. Photoinduced behaviour of the NIRIM1 EPR centre favours the interstitial Ni_i^+ model for this defect and suggests that the $Ni_i^{0/+}$ level is located at 1.98 ± 0.03 eV below the conduction band. In N-doped diamond, Ni_i is more likely to appear in the neutral state, undetectable by EPR, whereas at substitutional sites Ni_s^- is revealed. Observation of a strong AB2 EPR signal photoquenching and simultaneous detection of different spectral dependencies of the EPR intensity for other defects determine an electron photoionization energy of 1.67 ± 0.03 eV for the AB2. The implications of the obtained data for the identification of the AB defects' structure are discussed. Our study shows that Ni defects exhibit a weak electron–lattice interaction. The importance of the stronger spin–orbit coupling in these centres as compared to other defects in diamond is discussed. Assuming direct intercentre charge transfer from N_s, a theoretical description of the photoionization kinetics is proposed to explain the observed photoresponse of Ni defects.

1. Introduction

The unique physical properties of diamond make it an attractive subject of research from the fundamental and technological point of view [1]. The identification and characterization of

[3] Present address: Institute of Physics and Astronomy, University of Aarhus, DK-8000 Aarhus, Denmark.

point defects is still a primary focus of research as they influence the performance of diamond in several applications. An overview of the current problems concerning the research of point defects in diamond was given by Davies [2]. Nitrogen is the most common impurity in natural and synthetic high pressure and high temperature (HPHT) diamond, as isolated substitutional N_s and substitutional pairs (*A*-centres). As-grown HPHT diamonds incorporate N mostly in the N_s form, both neutral (N_s^0: P1 electron paramagnetic resonance (EPR) centre) [3] and positively charged.

Now the study of the role of transition metals in diamond is one of the most focused areas of diamond research, since they are used as solvent/catalysts in the HPHT synthesis. EPR of diamond grown from a solvent of Ni enriched with ^{61}Ni ($I = \frac{3}{2}$, natural abundance 1.2%) has proven the existence of negatively charged substitutional Ni_s^- with spin $S = \frac{3}{2}$ (W8), giving rise to an isotropic line at $g = 2.0319$ [4, 5]. Furthermore, strong evidence for the formation of Ni-related defects in diamonds grown from Ni-containing solvents has been found in EPR studies [6–13]. Among these centres, the AB1–AB6 [6–8] and NE1–NE8 [12] defects appear in N-rich crystals, whereas the NIRIM1 and NIRIM2 are typically observed in samples with low N concentration [8, 13]. Such crystals are usually grown from a Ni solvent with nitrogen getters (e.g., Ti). The interest in the study of transition metals results also from the possible variety of energy levels that the different charge states of one defect may induce in the energy gap. In contrast to the appreciable amount of information concerning the formation conditions and structure of Ni centres, there is little knowledge on their energy levels. Concerning EPR centres, the latter may be determined through EPR measurements upon photoexcitation (photo-EPR). Photo-EPR studies of the W8, P1 and AB5 ($S = 1$) signals have shown that the W8 photoquenching reported in [14] is caused by the promotion of electrons to the conduction band, and that the AB5 induces a level at $E_c - 1.88$ eV in the gap [15]. The photo-EPR may also provide information about the electronic properties of EPR centres, like their relaxation upon ionization and their aptitude for capturing and recombining charge carriers.

This work reports photo-EPR studies on several Ni-related defects in HPHT diamond. A general description of the photoinduced EPR response of defects is given in section 3. In section 4, we present a detailed study of the temperature dependence of the Ni_s^- photoionization. In section 5, we investigate the optical behaviour of the NIRIM1, and based on this we discuss the most likely models for the NIRIM1 and enquire about its energy level in the gap. We study the photoionization behaviour of the AB EPR centres and discuss the implications of the obtained results for clarifying their structure in section 6. The small relaxation upon ionization exhibited by Ni defects is also discussed. In section 7, the role of N_s in the observed EPR photoresponse of Ni defects is put on view.

2. Experimental details

We used HPHT diamonds grown by the temperature gradient method at NIRIM, Japan, with Ni or Ni–Ti alloys as a solvent/catalyst. Some samples were annealed after growth at 1600 °C under a stabilizing pressure of 6 GPa. EPR was measured using a Bruker ESP 300E Q-band spectrometer with a cylindrical TE_{011} resonator. Temperatures in the range 4.2–150 K were achieved with a continuous flow helium cryostat. Photo-EPR experiments were performed in the Q-band due to the better resolution as compared to the X-band, enabling us to monitor non-overlapping lines, and due to the higher sensitivity taking into account the small size of the available samples. The use of the Q-band cryostat is also advantageous as it prevents any unintentional blackbody irradiation of the samples as all the resonator insert is kept at low temperature. By contrast, in the flow cryostat standardly used in the X-band, the cavity walls

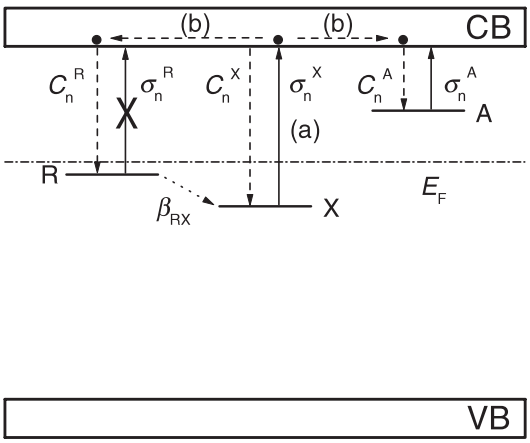

Figure 1. Diagram of the processes which may occur during an electron photoionization experiment of a given defect X in the upper half of the bandgap (E_g) for photon energies $h\nu < E_g/2$. Intercentre recharging through centres R is taken into account, whereas centres A behave only as electron trap levels. The photoinduction of an EPR signal may result from a direct photoionization mechanism (a) or, alternatively, may occur due to an indirect process of free carrier capture (b).

are kept at room temperature. Samples were slowly cooled down in the dark to guarantee thermal equilibrium before illumination. As a monochromatic light source we used light from a 100 W Xe lamp dispersed by a grating monochromator. For measuring photo-EPR, the samples were illuminated through a 0.4 mm optical fibre introduced into a homemade sample holder tube to be inserted into the cryostat. Light was then coupled into a second 0.4 mm optical fibre, at the end of which the spectral dependence of the photon flux was measured. The two fibres were connected when the samples were to be illuminated.

3. Photoionization kinetics

The photoionization energy of localized states is obtainable from the spectral dependence of the corresponding optical cross section $\sigma(h\nu)$. Among the existing methods of measuring $\sigma(h\nu)$, the saturation method is based on the analysis of the spectral distribution of the photoinduced changes ΔI_{EPR} produced on the EPR signal intensity I_{EPR} of a given centre [16]. The description of all processes occurring during the photoionization requires the solution of a complex system of kinetic equations that would consider all excitation, recharging and capture processes occurring at the levels involved. Godlewski [16] studied the photoionization processes which take place during a photo-EPR experiment and determined the relations between ΔI_{EPR} and σ for a few cases. However, the formalism does not account for the case of having simultaneously two different electron traps involving distinct physical processes. So, we consider the electron ionization of a defect X in the upper half of the bandgap with optical cross section σ_n^X and electron capture rate C_n^X for photon energies $h\nu < E_g/2$, see figure 1. N_X and n_X are the total concentration of defects X and the concentration of X in the non-ionized charge state, respectively. Taking into account direct intercentre electron transfer (recharging) by defects R ([R] $= N_R$) and free carrier capture by trap centres A ([A] $= N_A$), the kinetic equations describing the photoionization are:

$$\frac{dn_X}{dt} = -I\sigma_n^X n_X + C_n^X n(N_X - n_X) + \beta_{RX}(N_X - n_X)n_R, \tag{1}$$

$$\frac{dn_R}{dt} = C_n^R n(N_R - n_R) - \beta_{RX}(N_X - n_X)n_R, \tag{2}$$

$$\frac{dn_A}{dt} = -I\sigma_n^A n_A + C_n^A n(N_A - n_A), \tag{3}$$

$$\frac{dn}{dt} = I\sigma_n^X n_X - C_n^X n(N_X - n_X) - C_n^R n(N_R - n_R) + I\sigma_n^A n_A - C_n^A n(N_A - n_A). \tag{4}$$

Here n represents the concentration of free carries in the conduction band, I is the light intensity, and β_{RX} accounts for the transfer of electrons from R to X. n_R and n_A are the concentrations of defects R and A in the non-ionized charge state, respectively. Other symbols are explained in figure 1. In thermal equilibrium, the dark concentration of ionized trap centres would be N_A and the number of defects X in the photoinduced charge state would be zero. Equations (2)–(4) are derived assuming that centres R are not ionized by the incident light.

Assuming that a steady-state amount of excited electrons n is obtained on a very short timescale as compared with the time required to obtain a sensitive change in I_{EPR} [16], we may solve equation (4) independently, getting under stationary conditions:

$$n = \frac{\alpha_n^X N_X}{C_n^R(N_R - n_R^0) + C_n^A N_A}, \tag{5}$$

where $\alpha_n^X = I\sigma_n^X$ and n_R^0 is the dark concentration of non-ionized centres R. Substituting equation (5) in (2)–(4) and solving the set of equations for stationary conditions, the saturation values of the light induced changes produced in the occupancies of the non-ionized charge state of the centres X(Δn_X), R(Δn_R), and A(Δn_A) are given by

$$\Delta n_X = \frac{N_X}{N_R - (n_R^0 - \lambda)}\left\{\frac{\alpha_n^X}{2\beta_{RX}} + \frac{n_R^0 - \lambda}{2\Lambda} - \sqrt{\left(\frac{\alpha_n^X}{2\beta_{RX}}\right)^2 + \left(\frac{n_R^0 - \lambda}{2\Lambda}\right)^2 + \frac{\alpha_n^X[2N_R - (n_R^0 - \lambda)]}{2\Lambda\beta_{RX}}}\right\}, \tag{6}$$

$$\Delta n_R = -\frac{\alpha_n^X \Lambda}{2\beta_{RX}} - \frac{n_R^0 - \lambda}{2} + \sqrt{\left(\frac{\alpha_n^X \Lambda}{2\beta_{RX}}\right)^2 + \left(\frac{n_R^0 - \lambda}{2}\right)^2 + \frac{\alpha_n^X \Lambda[2N_R - (n_R^0 - \lambda)]}{2\beta_{RX}}}, \tag{7}$$

$$\Delta n_A = N_A \frac{\sigma_n^X C_n^A(\Lambda - 1)}{\sigma_n^A C_n^X + \sigma_n^X C_n^A(\Lambda - 1)}, \tag{8}$$

with

$$\Lambda = 1 + \frac{C_n^X N_X}{C_n^R(N_R - n_R^0) + C_n^A N_A} \qquad \text{and} \qquad \lambda = \frac{C_n^A}{C_n^R} N_A.$$

4. Substitutional nickel: W8 centre

In a recent work [15], the detection of two photoinduced effects on the W8 EPR signal was reported: a quenching of the signal for photon energies $h\nu > 2.5$ eV and a recovery for $h\nu > 3.0$ eV. From the intensity behaviour and as the sum of the two thresholds coincided with the 5.5 eV gap of diamond, they were interpreted as being the two complementary photoionization transitions (PTs) occurring at the $Ni_s^{-/0}$ defect level [15]. However, this assignment requires that the relaxation energy of the system upon electron removal/filling be very small.

Figure 2 shows schematically both PTs related to Ni_s in a configuration coordinate (CC) formalism [17]. Although this model had been originally created to describe transitions within localized states, it has been successfully applied to transitions between a localized state and a continuum of states [18–20]. In such an approach the electron–phonon interaction is generally

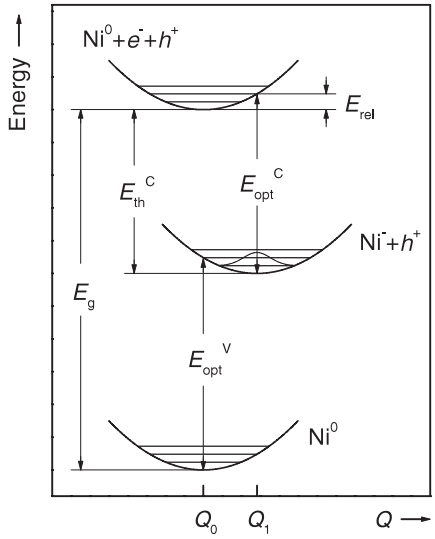

Figure 2. The CC scheme of the two complementary ionization transitions related to Ni_s. The assumption of a linear coupling in the electron–lattice interaction means that the CC diagrams will be made up of parabolas with the same curvature.

reflected in a temperature dependent broadening of the photoionization spectrum near the transition edge. Piekara *et al*, using a semiclassical approach, proposed an expression for the temperature dependent optical cross section σ [19],

$$\sigma(h\nu) = \frac{1}{\sqrt{\pi}} \int_{-\beta}^{\infty} \mathrm{d}z\, \mathrm{e}^{-z^2} \sigma_{\mathrm{el}}(E_{\mathrm{opt}}, h\nu + \Gamma z) \left(1 + \frac{\Gamma z}{h\nu}\right)^{-1}, \tag{9}$$

where

$$\Gamma = \hbar\Omega \sqrt{\frac{2(E_{\mathrm{opt}} - E_{\mathrm{th}})}{\hbar\omega} \coth\left(\frac{\hbar\omega}{2kT}\right)}, \tag{10}$$

and

$$\beta = \frac{h\nu - E_{\mathrm{opt}}}{\Gamma},$$

where σ_{el} is the purely electronic optical cross section. ω and Ω are the phonon frequencies of the ground and ionized states, respectively. Other symbols are explained in figure 2.

In order to determine the spectral dependence of the optical cross section σ of a definite PT from the spectral distribution of ΔI_{EPR}, we must find the relation between σ and ΔI_{EPR}. In the framework of the saturation method, our approach is based on the fact that I and σ always appear together (as $\alpha = I\sigma$) in the kinetic equations describing the photoionization. This leads to the same dependence of ΔI_{EPR} on both I and σ. When the measurements of the photoexcitation process are made under conditions of a linear dependence between ΔI_{EPR} and α, and if only one dominating photoionization is considered, ΔI_{EPR} also has a linear dependence on the corresponding σ. Making use of the results deduced in section 3, we will justify the linear behaviour of ΔI_{EPR} for small α, which is generally observed in our photo-EPR measurements.

Fixing the external magnetic field at the value giving the maximum intensity of the first derivative of the W8 line, we measured the time dependence of I_{EPR} upon an illumination

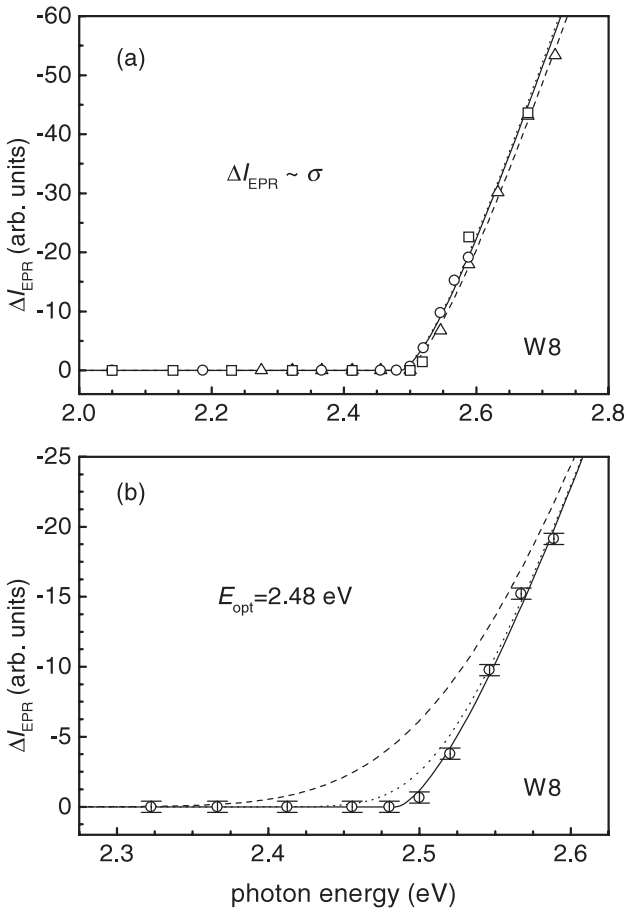

Figure 3. (a) Spectral dependence of the quenching of the W8 EPR signal produced by the PT with a threshold at 2.5 eV for 20 K (□), 60 K (△) and 150 K (○), and normalized to a constant photon flux. All curves result from the fitting of equation (9) to the experimental data for the temperatures: 20 K (solid curve), 60 K (dotted curve) and 150 K (dashed curve). (b) Normalized dependence of ΔI_{EPR} on $h\nu$ near the transition edge for $T = 150$ K. Experimental data are represented by circles and the solid curve results from fitting the experimental data by equation (9), which gives $E_{opt} = 2.48 \pm 0.02$ eV and $\Gamma = 0 \pm 0.01$ eV. Dashed and dotted curves are calculated using equation (9) with $E_{opt} = 2.48$ eV and $\Gamma = 0.1$ and 0.04 eV, respectively.

sequence with increasing $h\nu$. Figure 3(a) shows the spectral dependence of ΔI_{EPR} produced in the W8 line by the PT at 2.5 eV for three temperatures. The ΔI_{EPR} values were determined through fitting the I_{EPR} time dependence by exponential decay functions for each illumination window [15]. Here σ_{el} was substituted by the Lucovsky formula [21]

$$\sigma_{el}(E_{opt}, h\nu) \propto \frac{(h\nu - E_{opt})^{\frac{3}{2}}}{(h\nu)^3}. \tag{11}$$

The best fits of equation (9) to the experimental data for 20, 60 and 150 K are obtained with $E_{opt} = 2.49 \pm 0.03$, 2.49 ± 0.02, and 2.48 ± 0.02 eV, respectively, with Γ being virtually zero for all temperatures. In the temperature range of our measurements, the experimental data reveal no influence of the temperature on the spectral dependence of the PT at 2.5 eV. This is established by the vanishing broadening parameter Γ and a negligible variation in E_{opt}

resulting from the fitting. This is evidence for a small difference between the optical and thermal ionization thresholds $E_{rel} = E_{opt} - E_{th}$ for Ni_s^-, see figure 2.

Relying on the CC model and knowing the phonon frequencies ω and Ω, an upper limit E_{rel}^{max} for the relaxation energy can be estimated using equation (10). In figure 3(b) the spectral dependence of the photoquenching of the Ni_s^- EPR signal close to the transition edge is given. The experimental data were obtained at the maximum temperature used in the measurements (150 K), for this is the temperature at which we expect the strongest smoothing of the photoionization threshold. The variations of the optical cross section calculated by equation (9) using $E_{opt} = 2.48$ eV and the two Γ values 0.1 eV and 0.04 eV are also represented in figure 3(b). By introducing a non-zero Γ value, the model predicts a broadening of the photoionization threshold. As follows from figure 3(b), we may assume an upper detection limit of such broadening Γ_{max} of 0.04 eV. The 2.51 eV optical absorption band with a 16.5 meV phonon structure is believed to occur at the Ni_s^- centre [22]. In a linear coupling regime we get $\hbar\omega \simeq \hbar\Omega = 16.5$ meV, and substituting in equation (10) we obtain $E_{rel}^{max} = 0.02$ eV. The small value of E_{rel} is evidence for the weak electron–phonon coupling experienced by Ni_s in diamond.

5. The NIRIM1 centre

For studying the photoexcitation of the NIRIM1 spectrum (isotropic line at $g = 2.0112$) [13] we used diamonds grown using a Ni–Ti alloy. The samples contained typically ∼12 ppm of N_s^0 and ∼6 ppm of N_s^+ as measured by IR-absorption. Their EPR spectra evidenced the presence of the P1, W8 and NIRIM1 centres, with W8 and NIRIM1 concentrations of about 3 ppm and 0.2 ppm, respectively. The samples were successively irradiated with increasing $h\nu$ and consequent changes in the I_{EPR} measured. Figure 4 shows the spectral dependence of the changes produced on the NIRIM1 intensity. Also an increase of the P1 intensity and a slight decrease of the W8 intensity could be detected for $h\nu$ between 1.8 and ∼ 2.0 eV. In the same samples, the W8 intensity shows a strong decrease and a recovery for $h\nu > 2.5$ and 3.0 eV, respectively, in accordance with the observed in other crystals [15].

The detected changes in the signal's intensity should result from photoionization occurring on localized defect states, both directly on the centre whose signal is being monitored, or on other defects. In such an indirect process, electrons (holes) excited from a defect to the conduction band (valence band) are captured by the monitored centre. In both situations the ΔI_{EPR} values of the monitored centre depend on only one optical cross section σ, if we have non-overlapping PTs or only one dominant photoionization. The observation of simultaneous changes in the P1, W8 and NIRIM1 intensity for $h\nu < 2.0$ eV suggests that they have one and the same origin. Such a process does not involve either N_s^0 or Ni_s^- ionization, as their photoionization thresholds are $E_{opt} = 2.2$ [23] and 2.5 eV, respectively. Thus, the effect should involve ionization of another defect. The obvious candidates are NIRIM1 or another centre undetected by EPR. Moreover, the N_s^0 deep donor signal increase points out that the ionization involves electron excitation to the conduction band. The amount of NIRIM1 in the studied samples is rather low, so it cannot induce sufficient charge carriers that would be captured by N_s and Ni_s to produce the observed changes in their EPR signals. Thus, we conclude that the charge carriers must arise from another centre, with the observed photoinduced changes in the EPR defects concentration being a result of an indirect process (b), see figure 1. The observation of the P1 in the dark indicates that it is likely to have populated levels at $E_c - 1.8$ eV, as the thermal ionization energy of N_s^0 is found to be $E_{th} = 1.7$ eV [24], see figure 5. While for $h\nu < 2$ eV the NIRIM1 act as electron trap, the subsequent increase of its EPR intensity for $h\nu > 2$ eV is interpreted as resulting from its direct photoionization. Such an assumption is

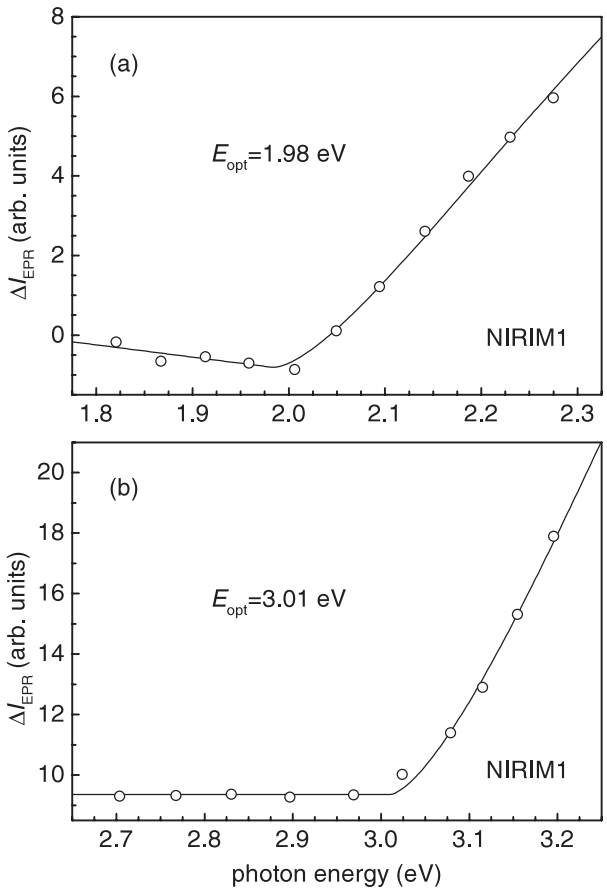

Figure 4. (a) Spectral dependence of the photoinduced changes in the intensity of the NIRIM1 spectrum, normalized to a constant photon flux. (b) Dependence of the enhancement of the NIRIM1 EPR signal intensity on $h\nu$ produced by the PT with a threshold at ∼3 eV. The circles present the experimental data and solid curves result from a fitting procedure to these data. For irradiation energies $h\nu > 2.4$ eV the ΔI_{EPR} values come to a saturation where an increase in the $h\nu$ does not produce any change in the EPR signal. The ΔI_{EPR} values for $h\nu > 2.6$ eV were measured relatively to this saturation value.

motivated by the fact that among the detected EPR centres, only NIRIM1 shows a photoinduced effect setting in at ∼2 eV. Fitting the dependence of ΔI_{EPR} for $h\nu > 2.0$ eV by equation (9), with σ_{el} given by equation (11), we obtain $E_{opt} = 1.98 \pm 0.03$ eV and $\Gamma = 0$ eV. It is likely that the process setting in at 3 eV and leading to a further increase of the NIRIM1 signal is the same as that which results in the detected enhancement of the W8 intensity. Here, the ionized state of NIRIM1 behaves as a trap level for holes that were excited from Ni_s^0. Fitting the ΔI_{EPR} dependence for 2.6 eV $> h\nu >$ 3.2 eV by equation (9), we obtain $E_{opt} = 3.01 \pm 0.05$ eV and $\Gamma = 0$ eV, in good agreement with the values determined for the W8 [15]. The observation of this effect corroborates the interpretation of the first onset at 1.98 eV as resulting from electron ionization.

According to the commonly applied Ludwig–Woodbury model [25], the simplest structures for the NIRIM1 which account for its spin $S = \frac{1}{2}$ and cubic symmetry are: (a) the previously proposed single interstitial Ni_i^+ with $3d^9$ configuration [13], and (b) the single substitutional Ni_s^+ ($3d^5$) in the low spin configuration. In the latter model the strong tetrahedral

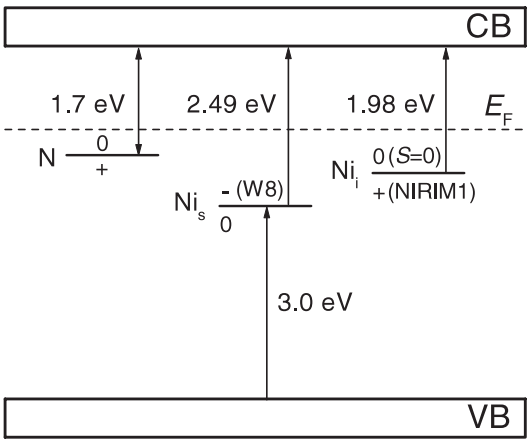

Figure 5. Diagram of the energy levels of Ni and N in diamond. The 1.7 eV level correspond to the thermal ionization energy of the N_s^0 donor (the optical one is 2.2 eV [23]), while the other levels correspond to optically determined thresholds. Due to the small Γ values of the Ni-related defects, the optically detected levels correspond to the thermodynamic filling levels. Thus, the comparison between the shown levels of the N_s and Ni-related defects is justified.

crystal field splits the 3d states into the subsets e and t_2, with e being well below t_2. The e subset is filled and one of the t_2 states is occupied with the fifth electron, giving rise to a $S = \frac{1}{2}$ state. In such a case, the NIRIM1 and W8 spectra would originate at the same defect with different charge states. With the $Ni_s^{0/+}$ level being located at $E_c - 1.98$ eV, the defect would correspond to a negative-U system, since the $Ni_s^{-/0}$ level is found to be located at $E_c - 2.48$ eV. In this situation the ionization of the Ni_s^- state would lead to the direct formation of the Ni_s^+ charge state. This is not in agreement with our experimental results, since we do not observe any increase of the NIRIM1 intensity for $h\nu > 2.48$ eV or the generation of this spectrum upon the photoquenching of the W8 line in samples where the NIRIM1 is absent in the dark. Thus, we favour the Ni_i^+ model for the NIRIM1 defect.

With the $Ni_i^{0/+}$ level located at $E_c - 1.98$ eV, we should expect that in HPHT diamond all Ni_i stay in the neutral state, since usually the concentration of N_s^0 is higher than that of N_s^+. The Ludwig–Woodbury model predicts for Ni_i^0 the $3d^{10}$ configuration with $S = 0$, undetectable by EPR. Thus, the Ni_i^+ state is observed in the dark due to fluctuations in the Fermi level resulting from inhomogeneities in the defects distribution, known to occur in these types of sample. The NIRIM1 is only observed in diamonds grown with a N getter or B-doped, where the N_s^0 concentration is much lower. We observe that the ratio between the concentration of N_s^0 and N_s^+ in samples which do not exhibit the presence of the NIRIM1 is in the range 3–5, whereas in samples where the NIRIM1 is observed this ratio decreases to values lower than 2. This means that the Fermi level is lowered in the latter type of crystal and the Ni_i^+ state becomes statistically possible to occur, though its concentration is usually quite low. The widespread idea that the interstitial Ni is more rarely formed than the substitutional form may result from the fact that Ni_i is normally incorporated in the neutral state that is undetectable by EPR. In contrast, Ni_s is easily detected as it is introduced in the negative charge state with an orbital singlet ground state with $S = \frac{3}{2}$.

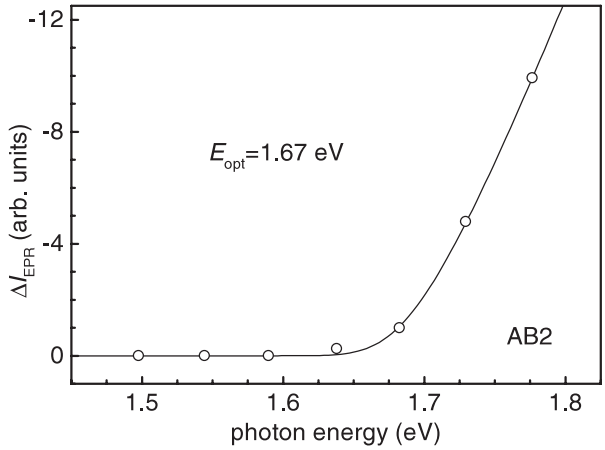

Figure 6. Spectral dependence of the photoinduced changes in the AB2 EPR intensity obtained under the same conditions as described in section 4 and normalized to a constant photon flux. Experimental data are represented by circles and the solid curve results from fitting the experimental data by equation (9).

6. The AB centres in diamond

The AB2 $S = \frac{1}{2}$ trigonal Ni-related defect was first observed in annealed HPHT diamonds grown from a pure Ni solvent [7]. A strong decrease of the AB2 EPR intensity upon illumination is observed. EPR spectra of the samples used exhibited the presence of P1, W8, AB1–AB6 and NE1-NE3 centres. IR-absorption estimates the concentrations of N_s^0, N_s^+ and A-centres as being typically 80, 25 and 250 ppm, respectively. Figure 6 shows the spectral dependence of the AB2 spectrum quenching. Taking σ_{el} as given by the Lucovsky formula, the fitting procedure leads to $E_{opt} = 1.67 \pm 0.03$ eV and $\Gamma = 0.03 \pm 0.03$ eV. Ionization of the AB5 centres was observed for $h\nu \geqslant 1.88$ eV [15]. The AB3 intensity decreased for $h\nu > 2.26$ eV, whereas the AB4 signal increased for $h\nu > 2.06$ eV [26]. No relevant changes were observed in the AB1 and AB6 EPR signal intensity.

Since only the AB2 exhibits a strong photoinduced effect setting in at 1.67 eV, we infer that the observed photoexcitation results from its direct ionization. The distinct photoexcitation thresholds detected for the AB2–AB5 centres should result from their direct ionization, because we do not expect that for a trap centre its ΔI_{EPR} would have a strong dependence on I, see equation (8), as is observed for the AB2–AB5. The observed PTs of the AB defects are likely to be related to the promotion of electrons to the conduction band, since E_F should be close to $E_c - 1.7$ eV in the samples used.

The AB3 and AB4, both with rhombic-I symmetry and no hyperfine structure [7], may in principle correspond to the same defect in different charge states. In such a situation, an increase of the AB4 concentration due to photoionization at $h\nu > 2.06$ eV would be accompanied by a corresponding decrease of the AB3. Though in the samples used the dark concentration of AB4 was approximately three times higher than that of AB3, we failed to observe such an opposite behaviour of their EPR intensities. Thus, the AB3 and AB4 spectra must belong to different defects.

According to the Ludwig–Woodbury model [25], the most likely structure for the AB5, consistent with its spin $S = 1$, is a substitutional Ni_s^{2-} ion, with the trigonal symmetry given by a Jahn–Teller distortion or a nearest-neighbour impurity, e.g., nitrogen [6]. In the case of a

Jahn–Teller effect, the W8 and AB5 spectra might correspond to the same defect in different charge states. In this case, through the photoionization of the AB5 for $h\nu > 1.88$ eV, we should detect an increase of the W8 intensity. This effect was not observed in our photo-EPR measurements, even in samples which show a significant AB5 concentration. Thus, we may rule out the hypothesis that the AB5 centre is a single Ni_s^{2-} ion.

It is interesting to note that all ionization transitions observed in our photo-EPR studies exhibit a photoexcitation with a sharp spectral onset, which is evidenced by the vanishing parameters Γ. Thus, a small relaxation energy E_{rel} appears to be a common characteristic of the Ni-related defects in diamond. In contrast, N_s^0 exhibits a rather strong relaxation upon ionization with $E_{rel} \approx 0.5$ eV [23, 24]. Small values of E_{rel} are indicative of a weak electron–lattice coupling of Ni in diamond. Huang–Rhys factors S for interacting vibrational modes, obtained from electron-vibrational spectra of Ni optical centres, also reveal modest electron–phonon coupling. For instance, the 1.40, 1.693, 1.883 and 2.51 eV optical features have factors S (and corresponding dominant phonon energy) of 1.6 (60 meV) [27], 1.3 (28 meV) [28], 0.7 (61 meV) [29] and ∼0.25 (16.5 meV) [22], respectively. This is possibly a result of the high localization of the defect wavefunction on the impurity. Moreover, the spin–orbit coupling, shown to be relatively strong in Ni defects (as derived from the deviations of the g-values from g_e), may play a predominant role in the stabilization of these defects, as compared to distortions due to the interaction between the electrons and the lattice vibrations.

7. The role of N in the photoionization kinetics

The deep N_s^0 donor acts as a charge compensator for other defects with even deeper acceptor levels, like Ni_s^-. In diamonds with an excess of nitrogen (with $[N_s] = N_N$), N_s coexists in thermal equilibrium in the neutral and positively charged states, with concentrations n_N and $N_N - n_N$, respectively. Even in diamonds grown with nitrogen getters, N is found to be the most abundant impurity and the Fermi energy E_F should be near $E_c - 1.7$ eV. This justifies the fact that most of the photoionizations observed in our photo-EPR measurements have energy thresholds E_{opt} above ∼1.7 eV. In this type of sample, N_s should also be the main path of direct charge transfer to other defects during photoionization. Such direct intercentre recharging was found to be quite efficient in deep defects in Si and, consequently, must be considered in the analysis of ionization experiments [30]. In the case of deep centres, this mechanism occurs by tunnelling and presupposes a non-vanishing overlap between the two defect wavefunctions. In our case this means a spatial correlation between N_s and Ni defects. The formation of Ni–N complexes in HPHT diamonds evidences the probability of such a correlation [12]. The intercentre charge transfer is responsible for some recovery of the EPR signals after switching off the illumination. Although this recovery was in some cases very small, it was always observed, proving the participation of these recharging processes.

Under these conditions, the changes produced by illumination in the population of the photoinduced charge state of a given centre X(Δn_X) have the form given by equation (7). For $\alpha_n^X/2\beta_{NX} \ll n_X^0$, with n_X^0 being the dark concentration of centres X in the non-ionized charge state, Δn_X has a linear dependence on α_n^X:

$$\Delta n_X \simeq -\frac{N_X}{(n_N^0 - \lambda)\beta_{NX}}\alpha_n^X \tag{12}$$

with

$$\lambda = \frac{C_n^A}{C_n^N}N_A.$$

Here n_N^0 is the dark concentration of P1 centres and C_n^N is the capture rate of electrons by N_s^+. For high α_n^X values, Δn_X no longer depends on α_n^X, i.e., ΔI_{EPR} does saturate as observed in our photo-EPR measurements,

$$\Delta n_X \simeq -\frac{N_X}{\Lambda} \tag{13}$$

with

$$\Lambda = 1 + \frac{C_n^X N_X}{C_n^N (N_N - n_N^0) + C_n^A N_A}.$$

In the case of the AB2–AB5 and NIRIM1, the approximation of negligible photoionization of the recharging centres R (see section 3) is justified, since N_s^0 is optically ionized only for $h\nu > 2.2$ eV [23]. The linear dependence on Δn_X is only observed in the case of a non-zero dark concentration of non-ionized centres R. In diamond, this is reflected by the observation of the P1 before illumination and justifies the observed linear dependence of ΔI_{EPR} on σ.

8. Conclusion

The photoexcitation properties of EPR centres in HPHT diamond were studied. The analysis of the temperature dependence of the W8 EPR signal photoquenching showed that the relaxation energy of Ni_s^- upon ionization should be less than ∼0.02 eV. This result corroborates the interpretation that the detected photoinduced effects with thresholds at 2.5 and 3.0 eV correspond to two complementary PTs involving Ni_s. Photoinduced changes of the NIRIM1 signal were studied and the two likely models for the NIRIM1 were discussed in the light of the photo-EPR data. Such an analysis favours the interstitial Ni^+ model, with the $Ni_i^{0/+}$ level being located at $E_c - 1.98 \pm 0.03$ eV. Our experimental results give an explanation for the widespread (and possibly erroneous) idea that Ni_i is less likely to be formed than Ni_s. In N-doped diamond, interstitial Ni is likely to appear in the neutral state, undetectable by EPR, whereas at substitutional sites Ni_s^- it is revealed. Photo-EPR data obtained in crystals exhibiting the presence of the AB1–AB6 defects were presented. Detection of a strong AB2 signal photoquenching, together with the observation of photoinduced changes on the other AB centres having different spectral dependencies, yielded an ionization energy of 1.67 ± 0.03 eV for the AB2. All detected optical ionization energies of the AB defects are likely to correspond to the electron promotion to the conduction band. Photo-EPR data show that the AB3 and AB4 rhombic-I centres cannot be different charge states of one and the same centre, and rule out the single Ni_s^{2-} model for the AB5. It is found that a small lattice relaxation upon ionization associated with a weak electron–phonon coupling is a common characteristic of Ni-related defects. This is possibly due to the stronger spin–orbit coupling experienced by these centres in contrast to other defects in diamond, e.g., N_s. Experimental evidence of direct intercentre charge transfer between N_s and Ni defects is given. This mechanism has largely been ignored due to the lack of experimental data.

Acknowledgments

The authors would like to thank H Kanda (National Institute for Materials Science, Japan) for supplying the samples. RNP acknowledges L Rino and J Coutinho for helpful discussion and thanks the Institute for Solid State Physics, TU-Berlin for its hospitality and financial support from FCT under contract PRAXIS XXI/BD/18405/98. The work was supported in part by *Acções Integradas Luso-Alemãs*, Project No A-13/99.

References

[1] Nazaré M H and Neves A J (ed) 2001 *Properties, Growth and Applications of Diamond (Series 26)* (London: INSPEC)
[2] Davies G 1999 *Physica* B **273/274** 15
[3] Smith W V, Sorokin P P, Gelles I L and Lasher G J 1959 *Phys. Rev.* **115** 1546
[4] Samoilovich M I, Bezrukov G N and Butuzov V P 1971 *JETP Lett.* **14** 379
[5] Isoya J, Kanda H, Norris J R, Tang J and Bowman M R 1990 *Phys. Rev.* B **41** 3905
[6] Neves A J, Pereira R, Sobolev N A, Nazaré M H, Gehlhoff W, Näser A and Kanda H 2000 *Diamond Relat. Mater.* **9** 1057
[7] Neves A J, Pereira R, Sobolev N A, Nazaré M H, Gehlhoff W, Näser A and Kanda H 1999 *Physica* B **273/274** 651
[8] Pereira R N, Neves A J, Gehlhoff W, Sobolev N A, Rino L and Kanda H 2002 *Diamond Relat. Mater.* **11** 623
[9] Pawlik T, Noble C J and Späth J-M 1998 *J. Phys.: Condens. Matter* **10** 9833
[10] Noble C J, Pawlik T and Späth J-M 1998 *J. Phys.: Condens. Matter* **10** 11781
[11] Mashkovtsev R I and Palyanov Y N 1999 *Solid State Commun.* **111** 397
[12] Nadolinny V A, Yelisseyev A P, Baker J M, Newton M E, Twitchen D J, Lawson S C, Yuryeva O P and Feigelson B N 1999 *J. Phys.: Condens. Matter* **11** 7357
[13] Isoya J, Kanda H and Uchida Y 1990 *Phys. Rev.* B **42** 9843
[14] Hofmann D M, Ludwig M, Christmann P, Volm D, Meyer B K, Pereira L, Santos L and Pereira E 1994 *Phys. Rev.* B **50** 17618
[15] Pereira R N, Gehlhoff W, Sobolev N A, Neves A J and Bimberg D 2001 *J. Phys.: Condens. Matter* **13** 8957
[16] Godlewski M 1985 *Phys. Status Solidi* a **90** 11
[17] Kelley C S 1972 *Phys. Rev.* B **6** 4112 and references therein
[18] Monemar B and Samuelson L 1978 *Phys. Rev.* B **18** 809
[19] Piekara U, Langer J M and Kruskowska-Fulde B 1977 *Solid State Commun.* **23** 583
[20] Kopylov A A and Pikhtin A N 1974 *Fiz. Tverd. Tela* **16** 1837 (Engl. transl. *Sov. Phys.–Solid State* 1975 **16** 1200)
[21] Lucovsky G 1965 *Solid State Commun.* **3** 299
[22] Nazaré M H, Lopes J C and Neves A J 2001 *Physica* B **308–310** 616
[23] Rosa J, Vaneck M, Nesladek M and Stals L 1999 *Diamond Relat. Mater.* **8** 721
[24] Walker J 1979 *Rep. Prog. Phys.* **42** 1605
[25] Ludwig G W and Woodbury H H 1962 *Solid State Physics* vol 13, ed F Seitz and D Turnbull (New York: Academic)
[26] Pereira R N, Gehlhoff W, Sobolev N A, Neves A J and Bimberg D 2001 *Physica* B **308–310** 589
[27] Davies G 1977 *Chemistry and Physics of Carbon* vol 13, ed P W Philips and P A Turner (New York: Dekker)
[28] Neves A J, Nazaré M H, Lopes J P and Kanda H 1999 *Physica* B **273/274** 636
[29] Nazaré M H and Rino L M 1993 *Mater. Sci. Eng.* B **21** 329
[30] Frens A M, Bennebroek M T, Zakrzewski A, Schmidt J, Chen W M, Janzén E, Lindström J L and Monemar B 1994 *Phys. Rev. Lett.* **72** 2939